Available online at www.sciencedirect.com
SCIENCE DIRECT
Icarus 181 (2006) 94–106
ICARUS
www.elsevier.com/locate/icarus

Near-infrared spectral observations and interpretations for S-asteroids 138 Tolosa, 306 Unitas, 346 Hermentaria, and 480 Hansa

Paul S. Hardersen [a,*,1] Michael J. Gaffey [a,1], Edward A. Cloutis [b,1], Paul A. Abell [c,1,2], Vishnu Reddy [a]

[a] *Department of Space Studies, Box 9008, University of North Dakota, Grand Forks, ND 58202, USA*
[b] *Department of Geography, Room 5L13, University of Winnipeg, Manitoba, Canada*
[c] *Planetary Astronomy Group, Astromaterials Research and Exploration Science, NASA Johnson Space Center, Mail Code SR, Houston, TX 77058, USA*

Received 27 April 2005; revised 31 August 2005

Available online 20 December 2005

Abstract

Near-infrared (∼0.7 to ∼2.5 μm) spectra of S-asteroids 138 Tolosa, 306 Unitas, 346 Hermentaria, and 480 Hansa suggest the presence of variable amounts of orthopyroxene ± clinopyroxene ± olivine ± plagioclase feldspar on the surfaces of these asteroids. The spectra of these asteroids were compared to laboratory mineral mixtures of orthopyroxene, clinopyroxene, and olivine [Singer, R.B., 1981. J. Geophys. Res. 86 (B9), 7967–7982; Cloutis, E.A., 1985. Master's thesis]. The band parameters (band centers, band areas) were quantified and temperature-corrected [Moroz et al., 2000. Icarus 147, 79–93; Gaffey et al., 2002. In: Bottke Jr., W.F., Cellino, A., Paolicchi, P., Binzel, R.P. (Eds.), Asteroids III. The University of Arizona Press, Tucson, pp. 183–204]. Each S-asteroid in this paper exhibits an overall spectral shape with band parameters that are inconsistent with ordinary chondrite near-infrared spectra and their inferred mineral abundances and/or pyroxene chemistries. 138 Tolosa displays a complex spectrum with a broad ∼1 μm absorption feature that displays a double Band I minimum, a well-defined absorption at ∼1.3 μm, and a broad, but weak absorption in the ∼2 μm region. Although different interpretations exist, the Tolosa spectrum is most consistent with a ∼60/40 mixture of Type B clinopyroxene and orthopyroxene. Spectra of 306 Unitas suggest a surface with variable amounts of low-Ca pyroxene and olivine. Unitas is located in the S-(IV) and S-(VI) subtype regions in Gaffey et al. [1993. Icarus 106, 573–602]. 346 Hermentaria exhibits a complex, broad Band I absorption feature and a weak Band II feature, which suggests a ∼50/50 mixture of clinopyroxene and orthopyroxene. Hermentaria is classified as an S-(III). Spectra of 480 Hansa suggest a dominant low-Ca pyroxene component with lesser amounts of olivine. Based on these characterizations, these four S-asteroids should not be considered as potential ordinary chondrite parent bodies. Furthermore, these results suggest that these S-asteroids experienced at least partial melting temperatures [$T \geqslant$ ∼950 °C: Gaffey et al., 1993. Icarus 106, 573–602; Keil, K., 2000. Planet. Space Sci. 48, 887–903] during the formation epoch in the early Solar System. Continuing spectroscopic investigations will discern the relative abundance of chondritic and thermally-evolved objects among the S-type asteroids that have survived since the formation epoch ∼4.56 billion years ago.
© 2005 Elsevier Inc. All rights reserved.

Keywords: Asteroids, composition; Mineralogy; Spectroscopy; Thermal histories

1. Introduction

Detailed near-infrared (NIR; ∼0.7–2.5 μm) spectroscopic investigations of asteroids have traditionally occurred at a relatively slow pace, with fewer than ∼100 asteroids with well-characterized mineralogies appearing in the literature through the year 2000. This slow pace has limited our understanding of asteroids and has allowed important hypotheses to avoid rigorous testing for many years (i.e., ordinary chondritic vs a thermally-evolved asteroid population, the nature of aster-

* Corresponding author. Fax: +1 (701) 777 3711.
E-mail address: hardersen@space.edu (P.S. Hardersen).
[1] Visiting astronomer at the Infrared Telescope Facility, which is operated by the University of Hawaii under Cooperative Agreement No. NCC 5-538 with the National Aeronautics and Space Administration, Office of Space Science, Planetary Astronomy Program.
[2] National Research Council Associate.

0019-1035/$ – see front matter © 2005 Elsevier Inc. All rights reserved.
doi:10.1016/j.icarus.2005.10.003

oids with "featureless" spectra, space weathering, etc.). High-quality, high signal-to-noise ratio (SNR) asteroid visible and near-infrared (VNIR) reflectance spectra are vital for the extraction of quantitative spectral parameters that allow strong constraints to be placed on an asteroid's surface mineralogy (Gaffey et al., 2002). High-SNR VNIR spectra also reveal subtle complexities in absorption features that indicate the presence of multiple major minerals on asteroid surfaces.

With the relatively recent introduction of the current generation of low-resolution, near-infrared spectrographs (TNG: Baffa et al., 2001; Subaru: Motohara et al., 2002; IRTF/SpeX: Rayner et al., 2003, 2004), the number of VNIR asteroid observations extending to ∼2.5 μm is increasing, which is likely to continue in the coming years (Goldader et al., 1991; Granahan et al., 1994; Bus et al., 2001; Burbine and Binzel, 2002; Bus and Binzel, 2002; Dotto et al., 2003; Izenberg et al., 2003; Kelley et al., 2003; Binzel et al., 2004; Birlan et al., 2004; Clark et al., 2004; Duffard et al., 2004; Hardersen et al., 2004; Rivkin et al., 2004; Sasaki et al., 2004; Sunshine et al., 2004; Abell et al., 2005a, 2005b; Hardersen et al., 2005; Reddy et al., 2005). This trend suggests that our understanding of asteroids may evolve at a faster rate in the future with more workers studying the large variety of scientific questions that relate to asteroids and the early Solar System.

The link between the ordinary chondrites and the S-asteroid population in the main-belt has been a long-running research question within the asteroid community (Gaffey et al., 1993, and references therein; Chapman, 1996; Meibom and Clark, 1999).

Related questions involve the fraction of S-asteroids that have ordinary chondritic compositions and the potential linking of those asteroids to specific types of ordinary chondrites (H, L, LL) (Gaffey and Gilbert, 1998). These questions are not only important for understanding the macroscopic nature of the S-asteroid population, but also for providing much-needed insight into the mechanism that drove the early Solar System heating event.

The terrestrial meteorite record clearly shows that most meteorite parent bodies were strongly modified by a short-lived heating event that occurred in the early Solar System (Keil, 2000), but questions remain as to the extent of this heating, the mechanism(s) involved, and how that heating affected the main-belt asteroid parent bodies as a function of heliocentric distance and body size. Two main hypotheses—^{26}Al radiogenic heating and T-Tauri induction heating—are usually invoked to explain the large number of achondritic and iron meteorite types and their presumed parent bodies (Urey, 1955; Herbert and Sonett, 1979; Herbert, 1989; Herbert et al., 1991; Grimm and McSween, 1993; Shimazu and Terasawa, 1995; McSween et al., 2002). A more accurate knowledge of the distribution of igneous (partly or fully differentiated) and chondritic (undifferentiated) asteroids in the main belt—of all taxonomic types—will better constrain the primordial heating pattern which will allow the likely heating mechanisms to be tested. It would also constrain models of the relative abundances of igneous and ordinary chondritic S-asteroids.

S-asteroids with relatively well-constrained mineralogic and geologic interpretations can be found in Gaffey (1984), Burbine et al. (1992), Gaffey et al. (1993), Reed et al. (1997), Gaffey and Gilbert (1998), Izenberg et al. (2003), and Sunshine et al. (2004). Based on these results, ∼49 (∼18%) of the first ∼280 S-asteroids (as defined by Tholen, 1984; Tholen and Barucci, 1989) have received more than cursory observations and interpretations. There is clearly a need to obtain, reduce, and interpret additional asteroid spectra, which will constrain individual asteroid surface mineralogies and allow application of their interpretations to questions involving the nature of the early Solar System.

2. Observations and data reduction

This paper presents results from observations of four S-asteroids (138 Tolosa, 306 Unitas, 346 Hermentaria, and 480 Hansa) that were observed in October 2001, March 2002, and/or October 2004. All observations were conducted using the SpeX near-infrared spectrograph (Rayner et al., 2003) at the NASA Infrared Telescope Facility (IRTF) on Mauna Kea, Hawaii. SpeX was used in the low-resolution 'asteroid' mode with the 0.8″-wide slit, which produces a spectral resolution of ∼94. Table 1 includes observational information for each ob-

Table 1
Observational information for 138 Tolosa, 306 Unitas, 346 Hermentaria, and 480 Hansa

Asteroid	Date	Start time (UT)	Total # of spectra	Right ascension	Declination	V (mag)	Airmass	Phase angle
138 Tolosa	10/10/2001	11:52	6	$0^h\ 3^m\ 30.73^s$	−4°18′19.8″	11.42	1.463	8.435°
306 Unitas	10/7/2001	13:12	10	$2^h\ 4^m\ 10.60^s$	0°33′23.9″	11.73	1.197	8.271°
306 Unitas	10/9/2001	13:31	6	$2^h\ 2^m\ 29.03^s$	0°17′32.3″	11.69	1.294	7.463°
306 Unitas	10/10/2001	12:25	10	$2^h\ 1^m\ 39.77^s$	0°10′6.9″	11.68	1.127	7.104°
306 Unitas	10/2/2004	05:05, 05:49, 06:17	34	$18^h\ 6^m\ 42.66^s$	−20°39′28.0″	13.13	1.418–1.751	29.605°
306 Unitas	10/3/2004	05:02, 05:42	24	$18^h\ 8^m\ 27.16^s$	−20°42′45.6″	13.14	1.416–1.559	29.556°
306 Unitas	10/4/2004	04:45, 05:22, 05:53	34	$18^h\ 10^m\ 17.49^s$	−20°46′5.3″	13.15	1.381–1.630	29.503°
346 Hermentaria	3/22/2002	14:26	10	$13^h\ 13^m\ 13.39^s$	5°55′50.8″	11.65	1.382–1.458	5.752°
480 Hansa	10/9/2001	12:23	6	$0^h\ 6^m\ 50.90^s$	26°51′22″	12.19	1.373	8.951°

Notes. For the 10/2/2004 observations of 306 Unitas, three sets of observations were conducted at the times shown above. For the 10/3/2004 observations of 306 Unitas, two sets of observations were conducted at the times shown above. For the 10/4/2004 observations of 306 Unitas, three sets of observations were conducted at the times shown above. A single asteroid spectrum has an integration time of up to 120 s. Observations utilized the 0.8″ slit. For the observing runs discussed in this paper, an observational set consists of between 6 and 14 spectra.

Table 2
Physical and dynamical information for Asteroids 138 Tolosa, 306 Unitas, 346 Hermentaria, and 480 Hansa

Name	Diameter (km)[1]	Albedo[1]	a (AU)[2]	e[2]	i[2]	Period (h)[3]	Family[4]
138 Tolosa	45.50 ± 2.1	0.2699 ± 0.027	2.449	0.1622	3.21°	10.103	W 158, K 15, L&S For, A A82
306 Unitas	46.70 ± 2.3	0.2212 ± 0.023	2.358	0.1502	7.26°	8.75	Vesta, W 165, K 9
346 Hermentaria	106.52 ± 20.2	0.2189 ± 0.009	2.796	0.1027	8.75°	19.408	K 36
480 Hansa	56.22 ± 2.5	0.2485 ± 0.024	2.644	0.0469	21.30°	16.19	N/A

[1] Tedesco et al. (2002).
[2] Tholen (1999).
[3] 138 Tolosa: Harris (1996); 306 Unitas: Hainaut-Rouelle et al. (1995); 346 Hermentaria: Wang and Shi (2002); 480 Hansa: Deyoung (1994).
[4] PDS Small Bodies Node at: http://pdssbn.astro.umd.edu/nodehtml/sbdb.html.

Table 3
Asteroid, standard star, and solar analogue star information for the October 2001, March 2002, and October 2004 IRTF observing runs

Date	Asteroid	Standard star	Spectral type	Solar analogue star	Spectral type
10/10/2001	138 Tolosa	SAO 147237	G3V	SAO 147237	G3V
10/7/2001	306 Unitas	SAO 129706	G2V	–	–
10/9/2001	306 Unitas	SAO 129706	G2V	–	–
10/10/2001	306 Unitas	SAO 129706	G2V	–	–
10/2/2004	306 Unitas	HD 164263	G2V	–	–
10/3/2004	306 Unitas	HD 164263	G2V	–	–
10/4/2004	306 Unitas	HD 164263	G2V	–	–
3/22/2002	346 Hermentaria	SAO 120107	G5III	SAO 120107	G5III
10/9/2001	480 Hansa	SAO 53622	G2V	–	–

Notes. All stellar spectral classifications obtained from the Simbad Astronomical Database at: http://simbad.u-strasbg.fr/Simbad. Solar analogue stars were not used for 306 Unitas or 480 Hansa due to anomalous solar analog/standard star spectral slopes.

serving run, Table 2 lists physical and dynamical information for each asteroid in this paper, and Table 3 lists the asteroids, and their associated standard and solar analogue stars for each observing run.

Our observational strategy involves obtaining series (i.e., sets) of typically ∼6–20 spectra with maximum integrations of 120 s for each spectrum. Our spectra are not summed, or co-added, during the observations. The observations also employ a nodding sequence that alternates between two pre-defined slit positions that occur in the following sequence: *ABBAABBA*.... This is convenient because it allows efficient background sky subtraction during the data reduction process.

The data reduction process can be divided into a seven-step sequence. Initially, raw spectra are processed using the Image Reduction and Analysis Facility (IRAF: http://iraf.noao.edu). Subtracting *AB* spectral pairs to remove the sky signal, tracing the peak signal along each CCD image to remove slit curvature effects, manually defining an aperture to include the signal from each spectrum, and extracting and summing the spectra into one-dimensional arrays of flux values is accomplished.

The second step involves performing a wavelength calibration using ∼3–6 argon arc spectra acquired each night. Argon spectral lines of known wavelength are matched to individual CCD channels in each spectrum. The wavelength-channel data are then combined and a polynomial function is fit to the data, which allows conversion from channel number to wavelength value. All argon arc spectra for each night, and for the entire observing run, are compared for consistency. Consistent results have been obtained during all previous IRTF/SpeX observing runs (2001 to present) with variations between runs of $\leqslant 0.011$ μm.

The data are imported into the SpecPR spectral processing program (Clark, 1980; Gaffey, 2003). The major SpecPR reduction tasks include: (1) applying sub-pixel CCD channel shifts to all spectra to remove effects due to instrumental flexure and/or guiding variations, (2) deriving wavelength-dependent extinction coefficients from the nightly standard star observations, (3) dividing each asteroid and solar analogue star spectrum by flux values derived from the chosen group of extinction coefficients, (4) creating an average nightly spectrum for each asteroid and solar analogue star, and (5) applying the following ratio to produce an average, normalized reflectance spectrum for a single night:

$$\text{asteroid/Sun} = (\text{asteroid/standard star})/(\text{solar analogue star/standard star}). \quad (1)$$

Subsequent data analysis, as discussed in Cloutis et al. (1986), Gaffey et al. (2002), and Gaffey (2003, 2005), allow determination of absorption band centers and areas. These parameters, and the analysis of laboratory spectra of mineral mixtures, allow quantification of an asteroid's surface mafic mineralogy, relative mafic mineral abundances (orthopyroxene/clinopyroxene/olivine), and pyroxene mineral chemistry. This information also allows comparison of an asteroid's derived mineral abundances and/or chemistries with different meteorite types to determine any potential affinities.

3. Results

All four S-asteroids in this paper were observed as targets-of-opportunity during their observing runs and were not selected based on previous work or expectations of any particular

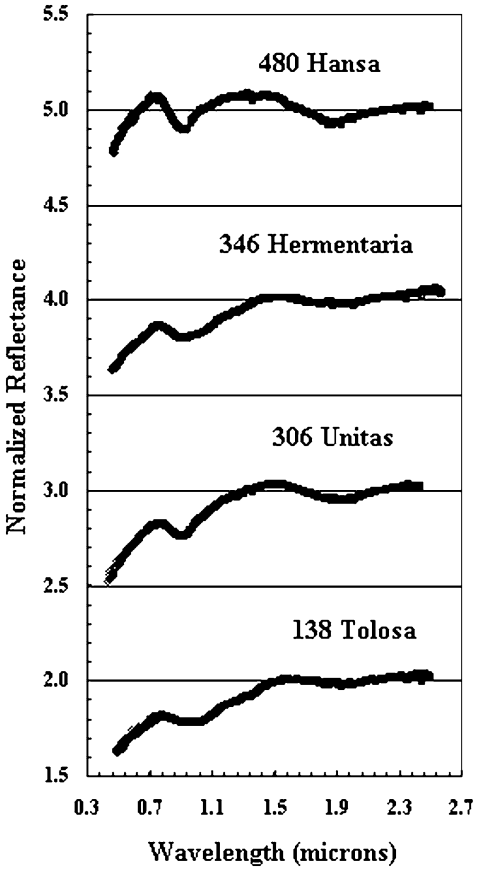

Fig. 1. Visible- and near-infrared reflectance spectra of 138 Tolosa, 306 Unitas, 346 Hermentaria, and 480 Hansa. Visible wavelength data are from the SMASS data sets (Xu et al., 1995; Bus and Binzel, 2002).

result. Each S-asteroid spectrum in this paper has been combined with SMASS data from Xu et al. (1995) or Bus and Binzel (2002).

3.1. 138 Tolosa

Six spectra of 138 Tolosa were obtained on October 10, 2001. Tolosa's average spectrum is shown in Figs. 1 and 2. This spectrum is notable for its very broad ∼1 μm absorption feature, a side-lobe feature at 1.3 μm, and a relatively weak feature at ∼2 μm. (Standard errors for the Tolosa data, as well as for our other spectra, are ∼0.005 μm.) The short wavelength (i.e., Band I) feature exhibits a double minimum at ∼0.93 and ∼1.03 μm. The linear continuum-removed Band I depth is ∼10%. This double feature bears a strong morphologic resemblance to some Type A and B clinopyroxene spectra (Cloutis and Gaffey, 1991; Schade et al., 2004). However, Type A clinopyroxene spectra (high-Ca pyx with only a Band I absorption) do not exhibit systematic band center variations with Fe^{2+} or Ca^{2+} content in their mineral structures and exhibit relatively constant band minima at ∼0.93 and ∼1.17 μm, of which the longer wavelength minimum is inconsistent with Tolosa's spectrum (Cloutis and Gaffey, 1991; Schade et al., 2004).

Several alternate mineralogical interpretations can possibly explain these ∼1- and ∼2-μm absorption features. The most probable option, based on available spectra of laboratory mineral mixtures, includes a mixture of Type B clinopyroxene (∼60%) and orthopyroxene (∼40%). PYX115 (Fig. 12 in Cloutis and Gaffey, 1991), which is an augitic pyroxene ($Wo_{37.1}En_{46.0}Fs_{16.9}$), has many similarities with Tolosa's spectrum and represents a pyroxene with discrete exsolution features (chemically distinct zones formed in a mineral by solid-state diffusion). Thus, the cpx/opx phases may represent exsolution lamellae from an original, homogeneous pyroxene that cooled slowly or may represent discrete clinopyroxene and orthopyroxene phases.

Two other possibilities include: (1) a mixed Type A–B clinopyroxene or (2) a mixture of ∼80% olivine with ∼20% orthopyroxene. The former option can reproduce the double minimum in the ∼1 μm region given appropriate amounts of Fe^{2+} in the M1 and M2 cation sites within the pyroxenes. However, the ∼2 μm feature will display a minimum longward of 2.0 μm, which is inconsistent with Tolosa's 1.96 μm Band II center. There is only a slight possibility that the latter option could reproduce Tolosa's complex spectrum. Laboratory mixtures of olivine and orthopyroxene have yet to produce near-infrared spectra with a double minimum in the 1 μm region (Singer, 1981; Cloutis, 1985), suggesting that this occurs rarely. Also, Tolosa does not exhibit a weak olivine feature at ∼0.65 μm (King and Ridley, 1987) or weak local maxima at 0.6- and 0.7-μm expected for this mineral mixture. The absence of these spectral characteristics suggests that olivine is at most a minor phase on Tolosa's surface.

The ∼1.3 μm feature can be attributed to olivine, Fe-rich orthopyroxene or plagioclase feldspar (Cloutis and Gaffey, 1991; Burns, 1993; Clark et al., 2003). There is no current method to definitively identify the mineral(s) causing this feature in an asteroid's reflectance spectrum. In olivine–orthopyroxene mixtures, this feature does not appear until a ∼50/50 mix of olivine and orthopyroxene (Cloutis, 1985). Natural orthopyroxenes with Fe content $\geqslant$ ∼40% can also produce an absorption feature at that wavelength region (Cloutis and Gaffey, 1991). Recent work by Klima et al. (2005) suggests that synthetic orthopyroxenes with $\geqslant$ ∼25% Fe can develop the same feature, which becomes stronger with increasing Fe content for natural and synthetic orthopyroxenes. (It is not yet clear whether this lower threshold for onset of the feature is real or an artifact of incomplete partitioning of iron between the M1 and M2 sites in the synthetic minerals.)

In pyroxenes, cations occur in two crystallographic positions, M1 and M2. In low calcium pyroxenes (LCP), both sites possess octahedral symmetry. The M1 site is smaller than the M2 site and is less distorted from octahedral symmetry than the larger M2 site (Papike, 1987; Burns, 1993). This applies to LCPs with both orthorhombic and monoclinic symmetry (Eeckhout et al., 2000). In high calcium pyroxenes (HCP) and pigeonites, the M1 site is more distorted and the M2 site is larger (and also distorted) than in LCPs. The M2 site is eight-coordinated when occupied by Ca^{2+}, but may reduce to six-coordination when this site is occupied by smaller cations such as Fe^{2+} and Mg^{2+}, resulting in an M2 geometry that is simi-

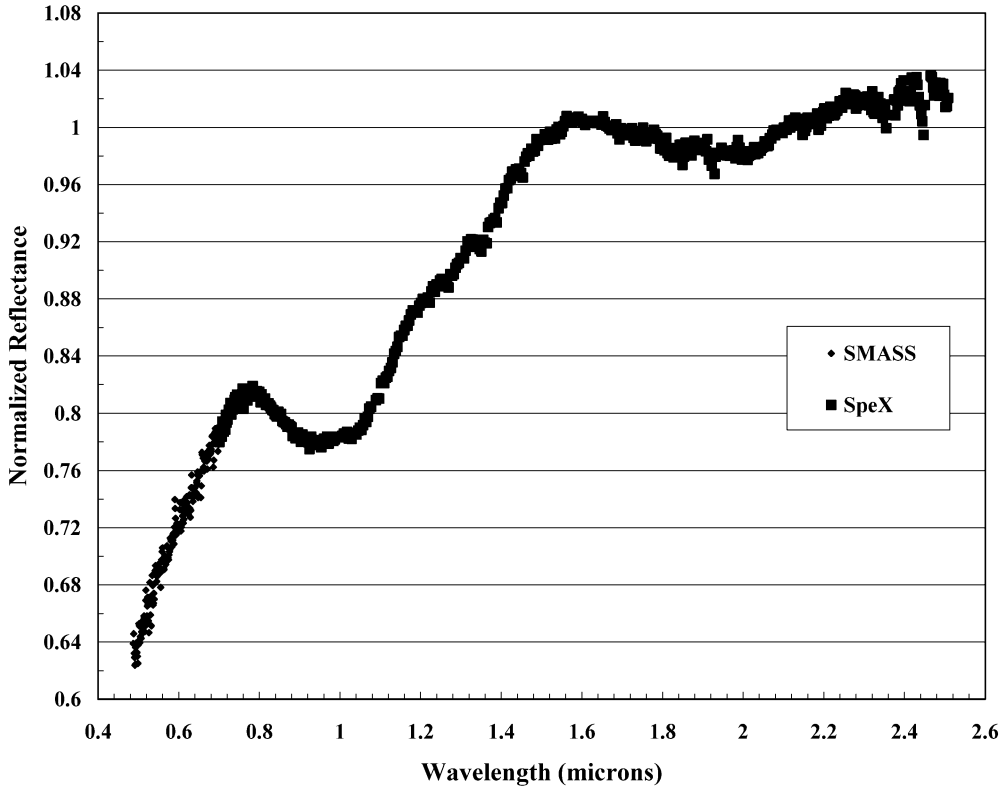

Fig. 2. Visible- and near-infrared reflectance spectrum of 138 Tolosa. Near-infrared data were obtained in October 10, 2001. Visible wavelength data are from the SMASS I data set (Xu et al., 1995).

lar to LCPs (Bancroft et al., 1967b; Papike, 1987; Burns, 1993; De Grave and Eeckhout, 2003).

Given differences in cation sizes, larger cations, such as Ca^{2+} and Fe^{2+} (in high spin configuration), will preferentially occupy the larger M2 site in both LCPs and HCPs, while smaller cations, such as Mg^{2+}, will preferentially occupy the smaller M1 site (Burns, 1993). When considering only Ca^{2+} and Fe^{2+}, Ca^{2+} has a stronger affinity than Fe^{2+} for the M2 site, thus Fe^{2+} will normally only occupy M2 sites in subcalcic HCPs. Appreciable Fe^{2+} will be present in the M1 site only when Ca^{2+} abundances (as well as other cations that strongly partition into the M2 site) are high ($\gtrsim Wo_{50}$), "forcing" Fe^{2+} to occupy the M1 site (Cloutis and Gaffey, 1991). There are also a number of other cations that are common constituents of pyroxenes. Mn^{2+}, Co^{2+}, Zn^{2+}, Cr^{2+}, and Na^{1+} show preferences for the M2 site (Burns, 1993). Ni^{2+}, Cr^{3+}, Al^{3+}, V^{3+}, Fe^{3+}, Ti^{3+}, and Ti^{4+} preferentially occupy the M1 site (Cloutis, 2002). Thus estimating M2 Fe^{2+} site occupancies in HCPs must take other cations besides Ca^{2+} into account (Schade et al., 2004).

In both LCPs and HCPs, Fe^{2+} is strongly, but normally not exclusively, partitioned into the M2 site. The degree of order/disorder is a function of temperature and can be used to estimate pyroxene cooling rates—rapidly cooled samples are more disordered (i.e., higher M1/M2 Fe^{2+} ratios) (Anovitz et al., 1988). Greater ordering is observed in metamorphic and plutonic samples, and less in volcanic samples, which relates to the speed of cooling. As a general observation, ~70–>90% of the Fe^{2+} will order into the M2 site for LCPs and pigeonites that are $<Fs_{50}$ (Bancroft et al., 1967a; Besancon, 1981; Anovitz et al., 1988; Molin, 1989; Domeneghetti and Steffen, 1992; Burns, 1993; Pasqual et al., 2000; Schlenz et al., 2001; Giuli et al., 2002; Tarantino et al., 2002; Zema et al., 2003). Pigeonites and LCPs show similar order–disorder behavior as a function of temperature, and Ca^{2+} in pigeonites seems to have little effect on Fe–Mg ordering (Pasqual et al., 2000). Fe^{2+} generally shows a slightly lower affinity for the M2 site in pigeonites than in LCPs (Burns, 1993). The M1/M2 Fe^{2+} site occupancy ratio generally increases with increasing Fe^{2+} content for $<Fs_{50}$ (Eeckhout et al., 2000). Site occupancy ratios are also affected by factors such as the concentration of trivalent cations. Greater abundances of trivalent cations generally lead to slight enrichments in M1 Fe^{2+} site occupancy (Saxena et al., 1987).

Complicating this picture is the fact that Ca-bearing LCPs, even those with a few percent Ca^{2+} or less, commonly exhibit either exsolution lamellae of Ca-rich phases or smaller Ca-rich exsolution zones (Guinier–Preston zones) (Lorimer and Champness, 1973; Champness and Lorimer, 1974; Nord, 1980; Camara et al., 2000; Zema et al., 2003). There may be a slight enrichment of Mg^{2+} in the Ca-rich regions, although Fe^{2+} abundances do not seem to correlate with Ca^{2+} content (Camara et al., 2000).

Spectrally, the presence of Fe^{2+} in the M1 site of LCPs results in two absorption bands in the 1-μm region due to crystal field transitions (Abu-Eid and Burns, 1976). Fe^{2+} in the M2 site gives rise to two absorption bands, one each in the 1- and 2-μm regions (Adams, 1974). Given that the M1 site is less distorted than M2, absorption bands due to Fe^{2+} in the M1 site will be

less intense than M2 absorptions for a specific Fe^{2+} content. The M1 bands, most clearly seen in the spectra of ferrosilite, occur near 0.93 and 1.17 μm (Burns, 1985, 1993; Rossman, 1980; Klima et al., 2005) or near 0.99 and 1.22 μm (Ross and Sowerby, 1996). The first of these bands is roughly coincident with the more intense M2 band (0.89–0.93 μm) (Burns, 1985; Ross and Sowerby, 1996). Whether these two M1 bands shift as a function of Fe^{2+} content, as is the case for the M2 bands (Cloutis and Gaffey, 1991), is currently unknown (e.g., Klima et al., 2005).

The Fe–Mg partitioning behavior for HCPs is similar to that for LCPs, although it appears that Fe^{2+} more strongly partitions into the M2 site than is the case for LCPs (Bancroft et al., 1967b; Brizi et al., 2000, 2001; De Grave and Eeckhout, 2003) and fully ordered HCPs (all Fe^{2+} in the M2 site) have been identified (Bancroft et al., 1971). The wavelength positions of the crystal field transition bands due to Fe^{2+} in the M1 site are at roughly 0.90–0.97 and 1.15–1.20 μm (Rossman, 1980; Cloutis and Gaffey, 1991) and the longer wavelength band may shift to longer wavelengths with increasing ferrous iron content (Schade et al., 2004). Fe^{2+} in the M2 site results in two absorption bands, one each in the 1 and 2 μm regions, similar to the case for LCPs, but the bands in HCPs are at longer wavelengths (Cloutis and Gaffey, 1991).

In summary, while absorption bands due to crystal field transitions in Fe^{2+} located in the M1 site are weaker than those for the M2 site for a given iron content, Fe^{2+} rarely partitions fully into the M1 site (with the notable exception of very Ca-rich HCPs). Increasing total Fe^{2+} content in pyroxenes also generally correlates with increasing M1 Fe^{2+} content. Consequently, M1 absorption bands become increasingly prominent as Fe^{2+} content increases in LCPs and HCPs. In HCPs, M1 absorption bands become increasingly prominent as both Fe^{2+} and Ca^{2+} contents increase.

Relating this back to Tolosa's surface mineralogy, high-Fe orthopyroxene seems unlikely because a high-Fe phase would cause the first band minima at ∼0.93 μm to shift to longer wavelengths than what is observed. Thus, Fe-rich orthopyroxene is a less likely option. Plagioclase feldspar is the third option and is an abundant mineral in basaltic meteorites such as eucrites, shergottites, and some angrites (Dodd, 1981; Burbine et al., 2001). Based on the uncertainty of the Fe-content of the orthopyroxene phase and the relatively minor olivine present on Tolosa's surface, we suggest that the ∼1.3 μm feature is probably caused by plagioclase feldspar.

Whether Tolosa represents a potentially basaltic or orthopyroxenite-like surface will largely depend on the actual relative abundance of plagioclase feldspar on the surface. There also seem to be a lack of meteorite analogues for this asteroid's spectrum and mineralogic characteristics. Regardless, it seems clear that Tolosa has experienced significant heating that led to partial or full differentiation of its parent body.

3.2. 306 Unitas

Spectra for 306 Unitas were obtained on six separate nights, three in October 2001 and three in October 2004. The attention given to Unitas was due to initial indications of significant spectral slope variations on opposite hemispheres in the 2001 spectra. However, re-observation in 2004 and re-analysis of the available data revealed probable instrumental artifacts, as discussed in Appendix A. The average nightly spectrum from 10/7/2001 in Fig. 1 (and all other Unitas spectra) was produced without using the solar analogue/standard star ratio in (1), due to the slope and band depth artifacts introduced into the final spectra.

The derived band centers for Unitas over the six nights are very consistent, with little apparent variation. Average band centers for all Unitas data are 0.92- and 1.92-μm, respectively. Individual Band I centers vary between 0.92- and 0.93-μm and Band II centers vary between 1.91- and 1.92-μm. Moroz et al. (2000) have shown that spectral parameters (i.e., band centers, band areas, etc.) of olivine–orthopyroxene mixtures can vary somewhat due to temperature differentials between spectra derived from laboratory samples (∼293 K) and asteroid surfaces (∼130–230 K: Moroz et al., 2000). Surface temperature estimates for the asteroids were calculated using the ThermFlux program written by M.J. Gaffey.[3] Sub-solar temperature estimates are 254 K for Tolosa, 250 K (2001) and 257 K (2004) for Unitas, 217 K for Hermentaria, and 233 K for Hansa.

Applying a linear relationship to the temperature changes in 50/50 mixtures of olivine and orthopyroxene (Moroz et al., 2000), the Unitas Band I center does not change while Band II increases by 0.01 μm. The uncorrected Unitas pyroxene chemistry is $\sim Wo_{5\pm4}Fs_{31\pm5}$ while the temperature-corrected chemistry is $\sim Wo_{4\pm4}Fs_{34\pm5}$, a variance smaller than the systematic uncertainties for the pyroxene equations in Gaffey et al. (2002). The Unitas data plots within the orthopyroxene region of the pyroxene band–band plot (Fig. 3). The uncorrected BAR values vary between ∼0.85 and ∼1.26; the temperature-corrected BAR values (which decrease by ∼5%) range from ∼0.81 to ∼1.20. This range suggests some variability in the relative orthopyroxene and olivine abundances. The opx/(opx + olivine) fraction varies from 0.40–0.55 using the calibration of Gaffey et al. (2002).

The Band I positions and BAR values place Unitas in the S-(IV) and S-(VI) regions in Fig. 4. This is consistent with the lack of an abundant high Ca-pyroxene phase due to its position near the olivine–orthopyroxene mixing line. The weak inflection in the ∼1.2- to 1.4-μm spectral region is likely caused by either plagioclase feldspar or olivine, since it is unclear whether natural orthopyroxenes can produce this feature given the estimated Fe content within the Unitas orthopyroxenes (Cloutis, 1985; Klima et al., 2005).

Unitas has a pyroxene chemistry that is inconsistent with the ordinary chondrites ($Fs_{34\pm5}$ vs $Fs_{15–26}$: Brearley and Jones, 1998) and an opx fraction (and variation) that is also mostly inconsistent with the ordinary chondrites. The variation in BAR values causes the Unitas opx fraction to slightly overlap the H-chondrite opx fraction. However, the apparent relative abun-

[3] Emissivity = 0.9 and beaming factor = 1.0 for most calculations. For the 2004 Unitas observations, a beaming factor of 0.75 was used due to the high phase angle of the asteroid during that observing run.

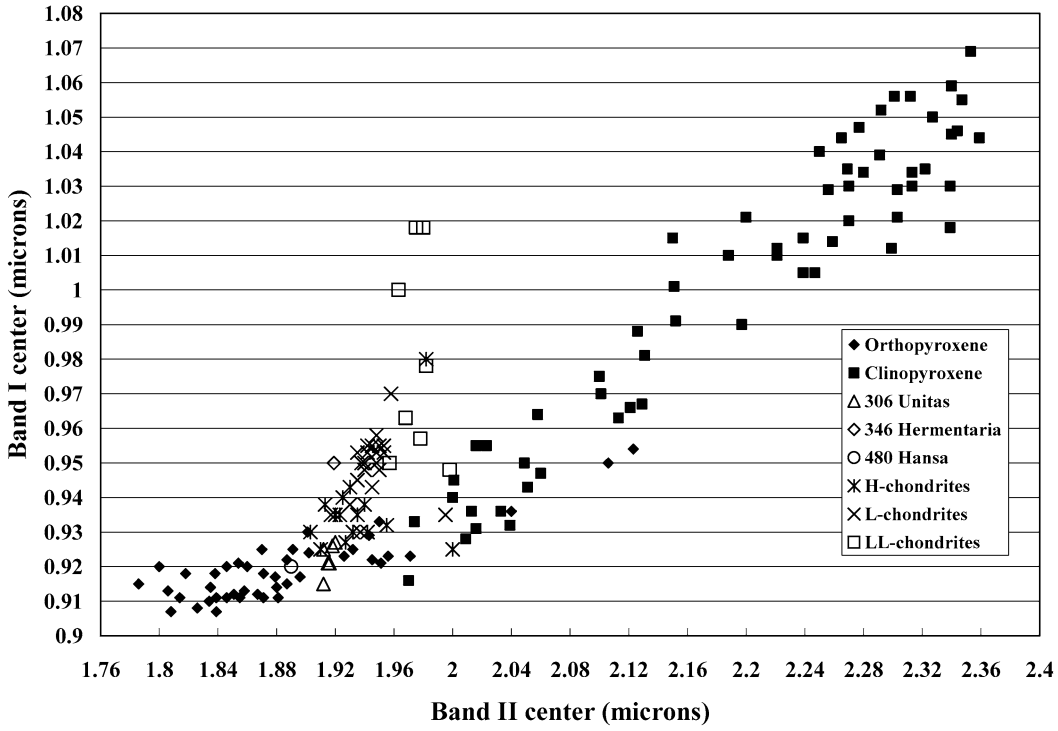

Fig. 3. Band–band plot from Adams (1974), as modified by Cloutis and Gaffey (1991). 306 Unitas and 480 Hansa plot within the orthopyroxene region. This suggests that these asteroids' surfaces are composed of orthopyroxene with sub-equal or lesser amounts of olivine. Data are also plotted for H, L, and LL ordinary chondrites for comparison. 346 Hermentaria plots above the pyroxene curve, which indicates the presence of an additional mineral phase(s). 138 Tolosa is not plotted because of the double minimum in the ∼1-μm region that will not produce a meaningful Band I center.

dance of orthopyroxene on Unitas is greater than that seen among the H-chondrites (37–48%: McSween et al., 1991).

Therefore, it seems unlikely that Unitas represents an ordinary chondrite assemblage. This asteroid may potentially represent a sub-surface crustal unit from a partially or fully-differentiated parent body. We envision Unitas possibly representing a relatively deep crustal unit adjacent to, and possibly gradational with, an olivine-rich mantle.

3.3. 346 Hermentaria

Ten spectra of 346 Hermentaria were obtained on March 22, 2002; the nightly average spectrum is shown in Fig. 1. Hermentaria exhibits a broad, asymmetric ∼1-μm feature with uncorrected band centers at 0.95- and 1.92-μm and a BAR of ∼0.43. Although spectral temperature corrections do not currently exist for two pyroxene mixtures, assuming an effect similar to 50/50 olivine–orthopyroxene mixtures will produce band centers of 0.95- and 1.94-μm, respectively, and a BAR of ∼0.39. These values would place Hermentaria among the S-(III) subtypes. The low BAR value and subsequent displacement above the band-band plot (Fig. 3) initially indicates a substantial olivine component. However, the shape and breadth of the Band I and II absorption features, as well as the band center data, are most consistent with a clinopyroxene–orthopyroxene mixture. This was confirmed by plotting Hermentaria's band parameters in Fig. 3 and applying a band displacement correction (Fig. 4: Gaffey et al., 2002). In this case, Hermentaria's BAR of ∼0.39 produces a Band I displacement of ∼0.07 μm, which drops Hermentaria's data point below the pyroxene trend line in Fig. 3. The simplest explanation is that clinopyroxene is present as a significant component and invalidates the Band I displacement calculation (which was derived for olivine–orthopyroxene mixtures). The presence of a Type A clinopyroxene component would also decrease the BAR value and invalidate an estimation of olivine and pyroxene abundances from the BAR value.

Hermentaria's spectrum could be explained entirely by a mixture of orthopyroxene and Type-A clinopyroxene. Alternatively, it could also be a mixture of orthopyroxene, Type-A clinopyroxene, and olivine, although olivine could not be the dominant component.

Hermentaria also exhibits an absorption in the ∼1.3 μm region, which is stronger than the Unitas feature, but weaker than Tolosa's. Olivine is an unlikely cause of this feature, leaving plagioclase feldspar and Fe-rich orthopyroxene as the other alternatives. In any case, it seems that Hermentaria's surface is dominated by a two-pyroxene mixture.

The presence of such assemblages strongly indicates an igneous history involving at least partial melting within the original parent body. However, more detailed interpretations are hampered by the ambiguity of the mineral producing the weak ∼1.3-μm absorption. The assignment of this feature will determine the primary petrologic interpretation for this asteroid. If the feature is due to plagioclase feldspar, then Hermentaria may have a predominantly basaltic composition. If Fe-rich orthopyroxene produces the feature, then Hermentaria may represent a subsurface crustal unit some distance away from any putative olivine mantle.

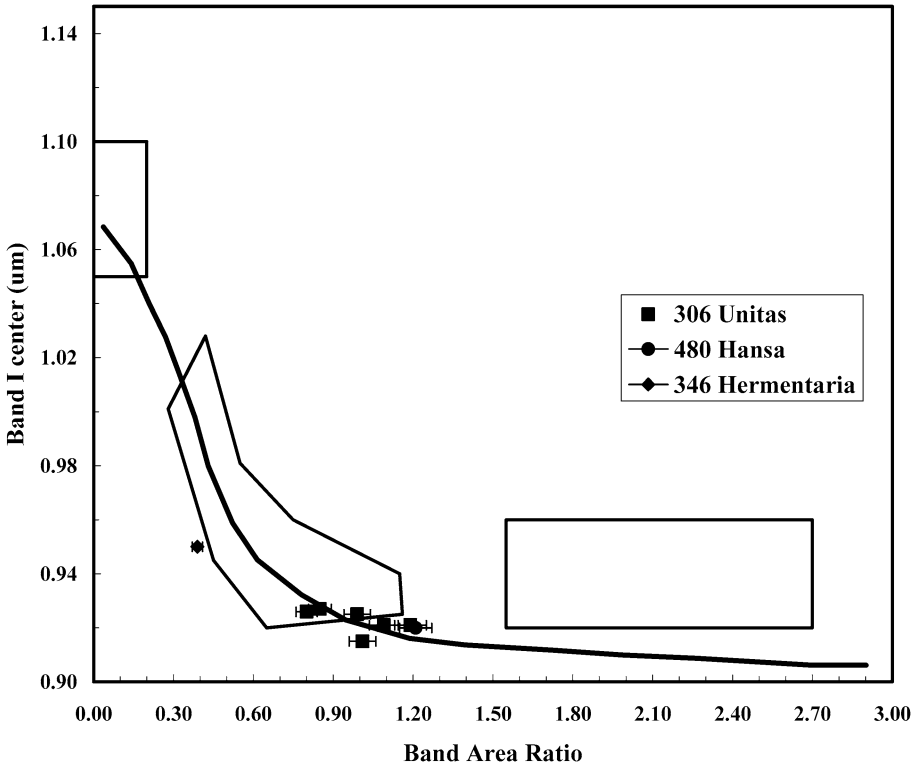

Fig. 4. Band I vs Band Area Ratio (BAR) plot, modified from Gaffey et al. (1993). 306 Unitas and 480 Hansa plot near the olivine–orthopyroxene mixing line, which indicates that these asteroids have surfaces dominated by these two mafic silicate minerals. 346 Hermentaria plots in the S-(III) subtype region from Gaffey et al. (1993).

3.4. 480 Hansa

Six spectra of 480 Hansa were obtained on October 9, 2001; the nightly average spectrum is shown in Fig. 1. Note that the telluric water vapor features (i.e., at 1.4- and 1.9-μm) are incompletely corrected, which introduces some uncertainty into the derived Band II center. Hansa's uncorrected band centers are 0.92- and 1.88-μm; the temperature corrected band centers are 0.92 and 1.89 μm (using the 50/50 opx/olivine mixture in Moroz et al., 2000). These correspond to pyroxene chemistries of $\sim Wo_{5\pm4}Fs_{19\pm5}$ and $\sim Wo_{5\pm4}Fs_{23\pm5}$ (Gaffey et al., 2002). Hansa plots directly in the orthopyroxene region in Fig. 3. The original and temperature-corrected BAR values are ~1.25 and ~1.21 (~3% decrease), which are very near the olivine–orthopyroxene mixing line in Fig. 4. This suggests a surface consisting primarily of orthopyroxene and olivine with minor or accessory clinopyroxene.

It is important to remember that orthopyroxene dominates the spectrum of olivine/orthopyroxene mixtures. More than 50% olivine is necessary to begin significantly shifting the Band I center to longer wavelengths (Singer, 1981; Cloutis et al., 1986). Hansa's surface orthopyroxene fraction is estimated at ~0.55 to ~0.57 (Moroz et al., 2000; Gaffey et al., 2002), which is larger than that measured in the ordinary chondrites from McSween et al. (1991). Unlike the previous three asteroids, Hansa's spectrum does not exhibit an obvious ~1.3-μm feature.

Hansa, which lacks any ~1.3 μm feature, may represent an orthopyroxenite-like cumulate layer with subordinate olivine. Although Hansa's pyroxene chemistry is consistent with ordinary chondrites, its opx fraction is too high and its positions in Figs. 3 and 4 are adjacent to—but not within—the ordinary chondrite data. The ordinary chondrite positions in Fig. 3 lie mostly above the pyroxene trend (L and LL chondrites, and some H-chondrites) due to a significant olivine component.

4. Discussion

A key challenge in S-asteroid research is determining which asteroids have affinities to the ordinary chondrites (OC) and which asteroids are likely to be thermally-evolved, meaning they have experienced at least partial melting temperatures ($T > 950\,°C$: Gaffey et al., 1993; Keil, 2000). This is an important question because although the ordinary chondrites dominate the terrestrial meteorite flux, there is no meteoritical data which requires more than three ordinary chondrite parent bodies. Previous spectral studies (Gaffey and Gilbert, 1998, and references therein) provides support to the delivery mechanism model which suggests that the high flux of ordinary chondrites is due to a few favorably located parent bodies rather than to ordinary chondrites being a common asteroid type.

Much mineralogic data is available from the large number of ordinary chondrites and ordinary chondrite (H, L, LL) mineralogy exhibits a relatively narrow range of mineral abundances and pyroxene mineral chemistries. Ordinary chondrites are dominated by varying abundances of olivine, orthopyroxene, and metal (in H- and L-chondrites) and troilite (FeS), along with minor to accessory amounts of albite, anorthite,

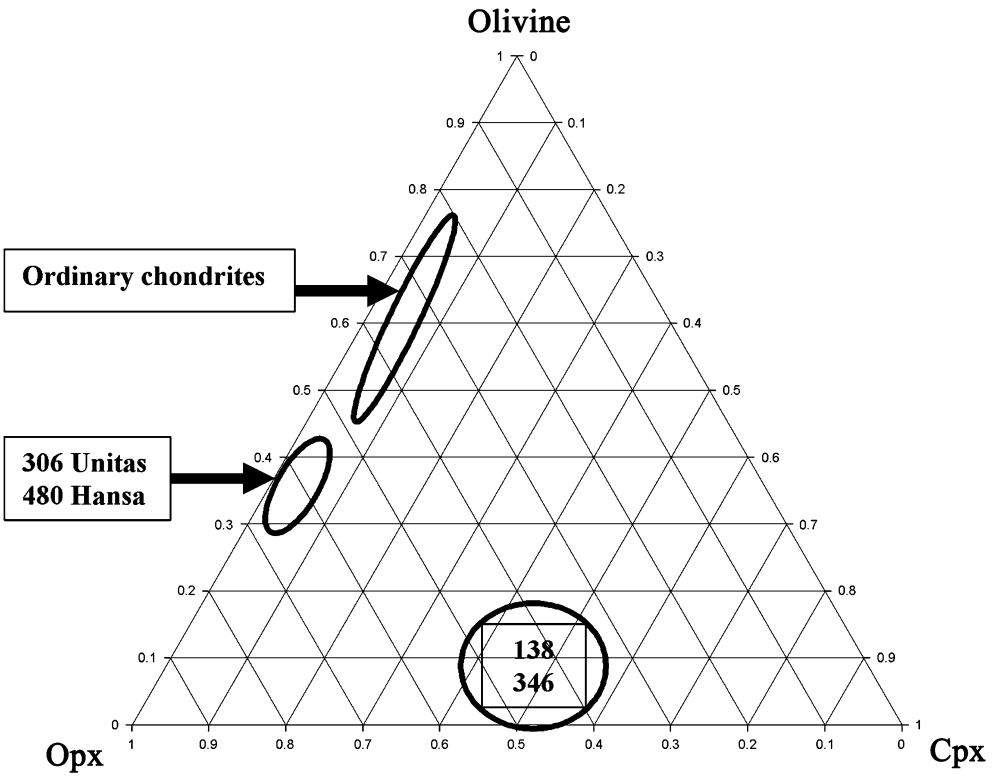

Fig. 5. A ternary diagram with orthopyroxene, clinopyroxene, and olivine end-members. Constraining the major mineral abundances allows asteroids and meteorite types to be plotted on diagrams of this type. This is an additional way to show the mineralogical similarities or differences between the meteorites types and the estimated mineral abundances on asteroid surfaces.

diopside, ilmenite, chromite, and apatite (McSween et al., 1991). Also, ordinary chondrite orthopyroxene chemistry spans a relatively narrow range, from $\sim Fs_{15–26}$ (Brearley and Jones, 1998).

By constraining asteroid surface mineralogic parameters, it is possible to identify S-asteroids with likely ordinary chondrite affinities. Conversely, it is also possible to exclude S-asteroids from the potential ordinary chondrite list when they exhibit characteristics that diverge from OC-like mineralogies and chemistries. A three-stage test can be applied to an S-asteroid's spectral and inferred mineralogic characteristics. Those S-asteroids that either: (1) exhibit major mineral abundances inconsistent with those found in ordinary chondrites, (2) have orthopyroxene chemistries outside the range found in ordinary chondrites, or (3) exhibit olivine–orthopyroxene relative abundance ratios and variations inconsistent with ordinary chondrites, can be excluded from consideration as analogues to ordinary chondrites. S-asteroids that pass these three tests can be considered potential ordinary chondrite analogues and should receive additional scrutiny. This methodology should be applied to the entire S-asteroid population as a vital first-step process to constrain those objects that are potentially chondritic and those that are thermally evolved.

All four S-asteroids in this paper exhibit spectral parameters and inferred surface mineral characteristics that are inconsistent with ordinary chondrites. 138 Tolosa and 346 Hermentaria include significant clinopyroxene phases, which are present in relatively minor abundance in ordinary chondrites. 138 Tolosa does not presently have any obvious meteorite analogues. As an S-(III) subtype, 346 Hermentaria is a candidate for the cpx/opx-bearing ureilites (Gaffey et al., 1993).

306 Unitas and 480 Hansa exhibit similar or greater relative proportions of orthopyroxene compared to the ordinary chondrites. The orthopyroxene fraction variations on Unitas, along with its derived pyroxene chemistries, provide additional evidence supporting an igneous interpretation for this asteroid. Based on the subtype classifications, potential meteorite analogues for Unitas include the opx-bearing ureilites, winonaites/IAB irons and the Steinback meteorite (Gaffey et al., 1993). Potential meteorite analogues for 480 Hansa include the winonaites/IAB irons and the Steinback meteorite.

The acapulcoites/lodranites have roughly 50/50 mixtures of olivine and low-Ca pyroxene, but their pyroxene mineral chemistries (acapulcoites: $Fs_{6.5–12.6}$; lodranites: $Fs_{3.7–13.8}$: Dodd, 1981; Mittlefehldt et al., 1998) are inconsistent with those for 306 Unitas ($\sim Fs_{34}$) and 480 Hansa ($\sim Fs_{23}$). Steinback and winonaite/IAB pyroxene chemistries (Steinback: $\sim Fs_{15}$; winonaites/IAB: $\sim Fs_{1–9}$: Dodd, 1981; Mittlefehldt et al., 1998) are also too magnesian to serve as possible analogues. Unitas and Hansa are spectrally dissimilar to ureilite spectra, have higher albedos compared to the ureilites, and usually contain differing relative abundances of orthopyroxene and olivine (Gaffey, 1976; Cloutis and Hudon, 2004). Thus, there also seem to be no obvious meteorite analogues for Unitas and Hansa.

The estimated relative abundances of olivine, clinopyroxene, and orthopyroxene for the four S-asteroids are plotted on

a ternary diagram in Fig. 5, as is the range encompassing the mafic silicates in ordinary chondrites. Orthopyroxene, clinopyroxene, and olivine abundances were derived from the normative mineral abundances in McSween et al. (1991) and then normalized to 100% (combined opx + cpx + olivine). The ordinary chondrite region encompasses the entire range of relative abundances for these minerals (from McSween et al., 1991), rather than simply using average relative mafic silicate abundances. 138 Tolosa and 346 Hermentaria plot within the same general region, while 306 Unitas and 480 Hansa plot together in a separate region. These regions are in significantly different areas of the ternary diagram as compared to the ordinary chondrites and highlight the mineralogical differences between these S-asteroids and the ordinary chondrites.

Another outstanding issue concerning S-asteroids is the cause(s) and consequence(s) of the increasing reflectance ('reddening') seen in many S-asteroid spectra compared to terrestrial meteorite spectra. Three of the four S-asteroids in this paper display that reddening, which is typically attributed to the presence of metal or the actions of some 'space weathering' effect (Clark et al., 2002). For these asteroids, significant metal content is an improbable explanation if these are nonchondritic objects. The only meteorite types with abundant metal include the ordinary (i.e., especially the H-type), CH, CR and enstatite chondrites, pallasites, mesosiderites, winonaites, lodranites, and the NiFe meteorites (Brearley and Jones, 1998; Mittlefehldt et al., 1998). None of the spectral data for the asteroids in this paper suggest an affinity to these meteorite types.

It is beyond the scope of this paper to consider the potential asteroid space weathering mechanisms and to determine if this mechanism is actually modifying asteroid surfaces sufficiently to cause the observed spectral changes. However, Hardersen et al. (2005, and references therein) note that space weathering simulations do not alter quantitative spectral band parameters that are used to constrain asteroid surface mineralogies and relative mineral abundances. Thus the interpretive approach used in the present paper is insensitive to space weathering effects, unlike curve-matching approaches which are very sensitive to space weathering-induced reddening of the overall spectrum and weakening of spectral features.

5. Conclusions and future work

S-asteroids 138 Tolosa, 306 Unitas, 346 Hermentaria, and 480 Hansa display spectral and mineralogic characteristics that are consistent with a variety of thermally- and petrologically-evolved ($T > 950\,^{\circ}C$) assemblages and are inconsistent with ordinary chondrite assemblages. Temperature effects on spectra acquired at significantly different temperatures (>140 K) have, at most, minor effects on absorption band centers and areas. No obvious meteorite analogues have been identified for the asteroids studied in this paper. More sophisticated interpretations are somewhat limited by the ambiguity of the ~1.3-μm feature that is present in three of the asteroids' spectra. Despite this limitation, we are able to successfully derive quantitative spectral parameters for each asteroid, compare this information with known spectral and mineralogic characteristics of ordinary chondrites, and test for ordinary chondrite candidates. Based on our results, we suggest that none of the asteroids discussed herein are analogues to ordinary chondrite meteorites.

Acknowledgments

Various portions of this work were supported under NASA Planetary Geology and Geophysics Grants NAG5-13792 and NNG04GJ86G and under NASA Near-Earth Objects Observation Program Grant NNG04GI17G [M.J.G.]. We thank Beth Clark and Tom Burbine for their constructive and useful comments that helped improve this manuscript.

Appendix A. Spex instrumental anomalies

During reduction of the 2001 Unitas data, we noticed significant slope and band depth variations (~few %) between the 10/9/2001 average Unitas spectrum and the average spectrum for 10/7/2001 and 10/10/2001, respectively. Initially, we thought these hemispherical variations might be due to a variety of physical processes occurring on the surface of Unitas (particle size variations, surface metal content on one hemisphere, space weathering, etc.). However, additional investigations revealed that the spectral variations were artificially created due to spurious variations in the solar analogue star/standard star ratios used in (1) to produce average nightly asteroid reflectance spectra.

When observing, we try to use standard stars and solar analogue stars of spectral type G2V whenever possible. When taking the ratio of two spectrally equivalent stars (i.e., G2V/G2V), we should observe a horizontal or near-horizontal line across the entire spectral interval (~0.7–2.5 μm). However, re-analysis of solar analogue and standard star data—all acquired from SpeX—from five different observing runs produce ratios that vary across different nights and different observing runs. Ratios using the same solar analogue and standard stars on different nights produce nonsystematic variations that deviate from theoretical expectations by varying amounts. The shorter (~0.7–1.3 μm) and longer wavelength (~2.2–2.5 μm) regions have been observed to deviate by up to ±20% from horizontal. See Fig. 6 for an example of these types of variations. When dividing an anomalous ratio into an asteroid/standard star ratio, spurious slopes and band areas can be imparted onto the spectrum. Due to this effect, we did not use the solar analogue/standard star ratios when producing the reflectance spectra for this paper.

It is important for workers who reduce their data in this manner to be aware of this potential problem. The deviations of the solar analogue/standard star ratios are of varying severity and do not always cause noticeable spectral slope variations. When the solar analogue/standard star ratio is significantly nonhorizontal, the most noticeable effect in the final asteroid reflectance spectrum is short- and/or long-wavelength slope changes of up to ~ ±5%. However, the slope changes are usually minor and inconsequential.

Band centers seem immune to this problem. We determined the band centers for Unitas using both the solar analogue/standard star ratios and without the ratio (simply using

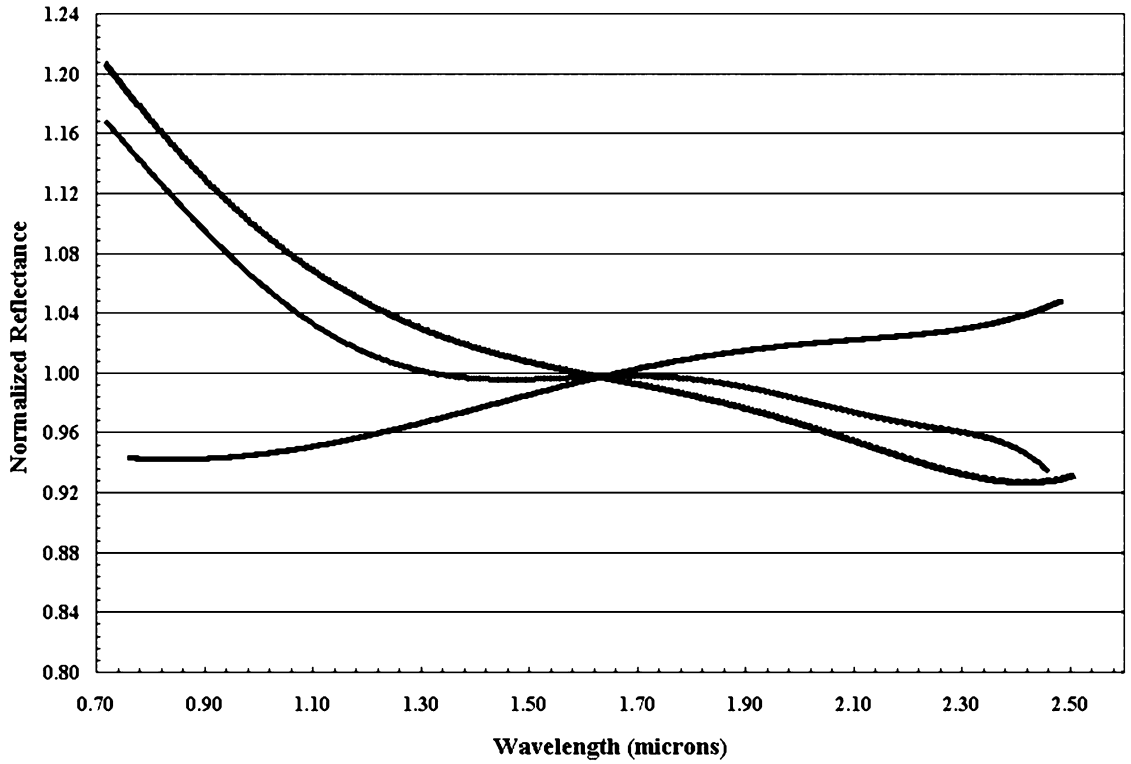

Fig. 6. Three curves representing ratios of a calibrated solar analogue star (SAO 31899) to SAO 129706. This plot displays nonsystematic slope variations using the same stars on different nights. When the slope deviations from horizontal are >10%, an observer must ensure that artificial slope and band depth variations are not introduced into the final asteroid spectrum. See the text for additional discussion of this issue.

the asteroid/standard star spectrum). Band I centers did not vary and Band II centers varied by ∼0.01 μm or less. There was some effect on the Band I and II areas (⩽20% variation), which affected the Band II/Band I area ratios (BAR: ⩽23% variation). The anomalous slopes can either increase or decrease the band depths and affect the resulting BAR values.

There are a few potential and, likely complementary, causes for these observed anomalies that may be generic to near-infrared arrays; thus, the variations may not only affect SpeX data. One of the first indications of problems in our data occurred when we noticed what can be described as a "short-wavelength flop" (widely varying slopes) of the data at wavelengths shortward of ∼1.4 μm. Rayner et al. (2004) report that "…due to the wavelength and time dependent effects of seeing, atmospheric refraction, and guiding, on the PSF, slit throughput is a function of wavelength and time. Consequently, spectral shape cannot be measured perfectly." While observing at the parallactic angle (Rayner et al., 2004) and using the Spextool data reduction package (Cushing et al., 2004; Vacca et al., 2004) will ameliorate most of these slope issues, they may not be completely eliminated.

What are the implications of these findings? First, workers must be diligent when reducing data to ensure that the average solar analogue star/standard star ratio for a given night generally meets theoretical expectations. If there is a deviation, then workers must determine if division by this ratio introduces anomalous slopes to the final asteroid spectrum. In many cases, there may not be a significant effect. Second, workers need to be aware of the intricacies of their particular instrument and of the general behavior of near-infrared arrays. That will allow workers to anticipate potential artifacts in near-infrared telescopic data and prevent most artifacts from reaching scientific publications. Such slope changes would be a potentially much more severe problem for investigators using curve-matching interpretive techniques rather than for investigators using band parameter interpretive techniques.

References

Abell, P.A., Fernandez, Y.R., Pravec, P., French, L.M., Farnham, T.L., Gaffey, M.J., Hardersen, P.S., Kusnirak, P., Sarounova, L., Sheppard, S.S., Narayan, G., 2005a. Physical characteristics of Comet Nucleus C/2001 OG_{108} (LONEOS). Icarus 179, 174–194.

Abell, P.A., Gaffey, M.J., Landis, R.R., Jarvis, K.S., 2005b. Compositional investigation of near-earth Asteroid 66063 (1998 RO1): A potentially undifferentiated assemblage. Lunar Planet. Sci. 36. Abstract 2283.

Abu-Eid, R.M., Burns, R.G., 1976. The effect of pressure on the degree of covalency of the cation–oxygen bonds in minerals. Am. Mineral. 61, 391–397.

Adams, J.B., 1974. Visible and near-infrared diffuse reflectance spectra of pyroxenes as applied to remote sensing of solid objects in the Solar System. J. Geophys. Res. 79, 4829–4836.

Anovitz, L.M., Essene, E.J., Dunham, W.R., 1988. Order–disorder experiments on orthopyroxenes: Implications for the orthopyroxene geospeedometer. Am. Mineral. 73, 1060–1073.

Baffa, C., Comoretto, G., Gennari, S., Lisi, F., Oliva, E., Biliotti, V., Checcucci, A., Gavrioussev, V., Giani, E., Ghinassi, F., Hunt, L.K., Maiolino, R., Mannucci, F., Marcucci, G., Sozzi, M., Stefanini, P., Testi, L., 2001. NICS: The TNG near infrared camera spectrometer. Astron. Astrophys. 378, 722–728.

Bancroft, G.M., Burns, R.G., Howie, R.A., 1967a. Determination of the cation distribution in the orthopyroxene series by the Mossbauer effect. Nature 213, 1221–1223.

Bancroft, G.M., Maddox, A.G., Burns, R.G., 1967b. Applications of the Mossbauer effect to silicate mineralogy. I. Iron silicates of known crystal structure. Geochim. Cosmochim. 31, 2219–2246.

Bancroft, G.M., Williams, P.G.L., Burns, R.G., 1971. Mossbauer spectra of minerals along the diopside–hedenbergite tie line. Am. Mineral. 56, 1617–1625.

Besancon, J.R., 1981. Rate of cation disordering in orthopyroxenes. Am. Mineral. 66, 965–973.

Binzel, R.P., Birlan, M., Bus, S.J., Harris, A.W., Rivkin, A.S., Fornasier, S., 2004. Spectral observations for near-Earth objects including potential target 4660 Nereus: Results from Meudon remote observations at the NASA infrared telescope facility (IRTF). Planet. Space Sci. 52, 291–296.

Birlan, M., Barucci, M.A., Vernazza, P., Fulchignoni, M., Binzel, R.P., Bus, S.J., Belskaya, I., Fornasier, S., 2004. Near-IR spectroscopy of Asteroids 21 Lutetia, 89 Julia, 140 Siwa, 2181 Fogelin and 5480 (1989YK8), potential targets for the Rosetta mission; remote observations campaign on IRTF. New Astron. 9, 343–351.

Brearley, A.J., Jones, R.H., 1998. Chondritic meteorites. In: Papike, J.J. (Ed.), Planetary Materials, vol. 36. Mineralogical Society of America, Washington, pp. 3-1–3-398.

Brizi, E., Molin, G., Zanazzi, P.F., 2000. Experimental study of intracrystalline Fe^{2+}–Mg exchange in three augite crystals: Effects of composition on geothermometric calibration. Am. Mineral. 85, 1375–1382.

Brizi, E., Molin, G., Zanazzi, P.F., Merli, M., 2001. Ordering kinetics of Mg–Fe^{2+} exchange in a $Wo_{43}En_{46}Fs_{11}$ augite. Am. Mineral. 86, 271–278.

Burbine, T.H., Gaffey, M.J., Bell, J.F., 1992. S-asteroids 387 Aquitania and 980 Anacostia—Possible fragments of the breakup of a spinel-bearing parent body with CO3/CV3 affinities. Meteoritics 27, 424–434.

Burbine, T.H., McCoy, T.J., Binzel, R.P., 2001. Spectra of angrites and possible parent bodies. Lunar Planet. Sci. 32. Abstract 1857.

Burbine, T.H., Binzel, R.P., 2002. Small main-belt asteroid spectroscopic survey in the near infrared. Icarus 159, 468–499.

Burns, R.G., 1985. Thermodynamic data from crystal field spectra. Rev. Mineral. 14, 277–316.

Burns, R.G., 1993. Mineralogical Applications of Crystal Field Theory. Cambridge Univ. Press, Cambridge.

Bus, S.J., A'Hearn, M.F., Bowell, E., Stern, S.A., 2001. (2060) Chiron: Evidence for activity near aphelion. Icarus 150, 94–103.

Bus, S.J., Binzel, R.P., 2002. Phase II of the small main-belt asteroid spectroscopic survey: The observations. Icarus 158, 106–145.

Camara, F., Doukhan, J.-C., Domeneghetti, M.C., Zema, M., 2000. A TEM study of Ca-rich orthopyroxenes with exsolution products: Implications for Mg–Fe ordering process. Eur. J. Mineral. 12, 735–748.

Champness, P.E., Lorimer, G.W., 1974. A direct lattice-resolution study of precipitation (exsolution) in orthopyroxene. Philos. Mag. 30 (8), 357–365.

Chapman, C., 1996. S-type asteroids, ordinary chondrites, and space weathering: The evidence from Galileo's fly-bys of Gaspra and Ida. Meteorit. Planet. Sci. 31, 699–725.

Clark, B.E., Hapke, B., Pieters, C., Britt, D., 2002. Asteroid space weathering and regolith evolution. In: Bottke Jr., W.F., Cellino, A., Paolicchi, P., Binzel, R.P. (Eds.), Asteroids III. The University of Arizona Press, Tucson, pp. 585–599.

Clark, B.E., Bus, S.J., Rivkin, A.S., Shepard, M.K., Shah, S., 2004. Spectroscopy of X-type asteroids. Astron. J. 128, 3070–3081.

Clark, R.N., 1980. A large-scale interactive one-dimensional array processing system. Publ. Astron. Soc. Pac. 92, 221–224.

Clark, R.N., Swayze, G.A., Wise, R., Livo, K.E., Hoefen, T.M., Kokaly, R.F., Sutley, S.J., 2003. USGS digital spectral library splib05a. USGS Open File Report 03-395.

Cloutis, E.A., 1985. Interpretive techniques for reflectance spectra of mafic silicates. Master's thesis. Planetary Geosciences Division, Hawaii Institute of Geophysics, University of Hawaii, Honolulu.

Cloutis, E.A., 2002. Pyroxene reflectance spectra: Minor absorption bands and effects of elemental substitutions. J. Geophys. Res. 107 (E6), doi:10.1029/2001JE001590.

Cloutis, E.A., Gaffey, M.J., Jackowski, T.L., Reed, K.L., 1986. Calibrations of phase abundance, composition, and particle size distribution for olivine–orthopyroxene mixtures from reflectance spectra. J. Geophys. Res. 91, 641–653.

Cloutis, E.A., Gaffey, M.J., 1991. Pyroxene spectroscopy revisited: Spectral-compositional correlations and relationship to geothermometry. J. Geophys. Res. 96, 22809–22826.

Cloutis, E.A., Hudon, P., 2004. Reflectance spectra of ureilites: Nature of the mafic silicate absorption features. Lunar Planet. Sci. 35. Abstract 1257.

Cushing, M.C., Vacca, W.D., Rayner, J.T., 2004. Spextool: A spectral extraction package for SpeX, a 0.8–5.5 micron cross-dispersed spectrograph. Publ. Astron. Soc. Pac. 116, 362–376.

De Grave, E., Eeckhout, S.G., 2003. ^{57}Fe Mossbauer-effect studies of Ca-rich, Fe-bearing clinopyroxenes. Part III. Diopside. Am. Mineral. 88, 1145–1152.

Deyoung, J.A., 1994. The light curve and period of the S-type minor Planet 480 Hansa. Minor Planet. Bull. 21, 33.

Dodd, R.T., 1981. Meteorites: A Petrologic-Chemical Synthesis. Cambridge Univ. Press, Cambridge.

Domeneghetti, M.C., Steffen, G., 1992. M1, M2 site populations and distortion parameters in synthetic Mg–Fe orthopyroxenes from Mossbauer spectra and X-ray structure refinements. Phys. Chem. Miner. 19, 298–306.

Dotto, E., Barucci, M.A., Leyrat, C., Romon, J., de Bergh, C., Licandro, J., 2003. Unveiling the nature of 10199 Chariklo: Near-infrared observations and modeling. Icarus 164, 122–126.

Duffard, R., Lazzaro, D., Licandro, J., de Sanctis, M.C., Capria, M.T., Carvano, J.M., 2004. Mineralogical characterization of some basaltic asteroids in the neighborhood of (4) Vesta: First results. Icarus 171, 120–132.

Eeckhout, S.G., De Grave, E., McCammon, C.A., Vochten, R., 2000. Temperature dependence of the hyperfine parameters of synthetic $P2_1/c$ Mg–Fe clinopyroxenes along the $MgSiO_3$–$FeSiO_3$ join. Am. Mineral. 85, 943–952.

Gaffey, M.J., 1976. Spectral reflectance characteristics of the meteorite types. J. Geophys. Res. 81 (5), 905–920.

Gaffey, M.J., 1984. Rotational spectral variations of Asteroid (8) Flora: Implications for the nature of the S-type asteroids and for the parent bodies of the ordinary chondrites. Icarus 60, 83–114.

Gaffey, M.J., 2003. Observational and data reduction techniques to optimize mineralogical characterizations of asteroid surface materials. Lunar Planet. Sci. 34. Abstract 1602.

Gaffey, M.J., 2005. The critical importance of data reduction calibrations in the interpretability of S-type asteroid spectra. Lunar Planet. Sci. 36. Abstract 1916.

Gaffey, M.J., Burbine, T.H., Piatek, J.L., Reed, K.L., Chaky, D.A., Bell, J.F., Brown, R.H., 1993. Mineralogical variations within the S-type asteroid class. Icarus 106, 573–602.

Gaffey, M.J., Gilbert, S.L., 1998. Asteroid 6 Hebe: The probable parent body of the H-type ordinary chondrites and the IIE iron meteorites. Meteorit. Planet. Sci. 33, 1281–1295.

Gaffey, M.J., Cloutis, E.A., Kelley, M.S., Reed, K.L., 2002. Mineralogy of asteroids. In: Bottke Jr., W.F., Cellino, A., Paolicchi, P., Binzel, R.P. (Eds.), Asteroids III. The University of Arizona Press, Tucson, pp. 183–204.

Giuli, G., Paris, E., Wu, Z., Mottana, A., Seifert, F., 2002. Fe and Mg local environment in the synthetic enstatite–ferrosilite join: An experimental and theoretical XANES and XRD study. Eur. J. Mineral. 14, 429–436.

Goldader, J.D., Tholen, D.J., Cruikshank, D.P., Hartmann, W.K., 1991. Galileo support observations of Asteroid 951 Gaspra. Astron. J. 102, 1503–1509.

Granahan, J.C., Fanale, F.P., Robinson, M.S., Carlson, R.W., Kamp, L.W., Klaasen, K.P., Weissman, P.R., Belton, M., Cook, D., Edwards, K., McEwen, A.S., Soderblom, L.A., Carcich, B.T., Helfenstein, P., Simonelli, D., Thomas, P.C., Veverka, J., 1994. A Galileo multi-instrument spectral analysis of 951 Gaspra. Lunar Planet. Sci. 25, 453–454.

Grimm, R.E., McSween Jr., H.Y., 1993. Heliocentric zoning of the asteroid belt by aluminum-26 heating. Science 259, 653–655.

Hainaut-Rouelle, M.-C., Hainaut, O.R., Detal, A., 1995. Lightcurves of selected minor planets. Astron. Astrophys. Suppl. 112, 125.

Hardersen, P.S., Gaffey, M.J., Abell, P.A., 2004. Mineralogy of Asteroid 1459 Magnya and implications for its origin. Icarus 167, 170–177.

Hardersen, P.S., Gaffey, M.J., Abell, P.A., 2005. Near-IR spectral evidence for the presence of iron-poor orthopyroxenes on the surfaces of six M-type asteroids. Icarus 175, 141–158.

Harris, A.W., 1996. Letters to the editor. IAPPP Comm. 65, 54.

Herbert, F., 1989. Primordial electric induction heating of asteroids. Icarus 78, 402–410.

Herbert, F., Sonett, C.P., 1979. Electromagnetic heating of minor planets in the early Solar System. Icarus 40, 484–496.

Herbert, F., Sonett, C.P., Gaffey, M.J., 1991. Protoplanetary thermal metamorphism: The hypothesis of electromagnetic induction in the protosolar wind. In: Sonett, C.P., Giampapa, M.S., Matthews, M.S. (Eds.), The Sun in Time. The University of Arizona Press, Tucson, pp. 710–739.

Izenberg, N.R., Murchie, S.L., Bell, J.F., McFadden, L.A., Wellnitz, D.D., Clark, B.E., Gaffey, M.J., 2003. Spectral properties and geologic processes on Eros from combined NEAR NIS and MSI data sets. Meteorit. Planet. Sci. 38, 1053–1077.

Keil, K., 2000. Thermal alteration of asteroids: Evidence from meteorites. Planet. Space Sci. 48, 887–903.

Kelley, M.S., Vilas, F., Gaffey, M.J., Abell, P.A., 2003. Quantified mineralogical evidence for a common origin of 1929 Kollaa with 4 Vesta and the HED meteorites. Icarus 165, 215–218.

King, T.V.V., Ridley, W.I., 1987. Relation of the spectroscopic reflectance of olivine to mineral chemistry and some remote sensing implications. J. Geophys. Res. 92, 11457–11469.

Klima, R.L., Pieters, C.M., Dyar, M.D., 2005. Pyroxene spectroscopy: Effects of major element composition on near, mid and far-infrared spectra. Lunar Planet. Sci. 36. Abstract 1462.

Lorimer, G.W., Champness, P.E., 1973. Combined electron microscopy and analysis of an orthopyroxene. Am. Mineral. 58, 243–248.

McSween Jr., H.Y., Bennett III, M.E., Jarosewich, E., 1991. The mineralogy of ordinary chondrites and implications for asteroid spectrophotometry. Icarus 90, 107–116.

McSween Jr., H.Y., Ghosh, A., Grimm, R.E., Wilson, L., Young, E.D., 2002. Thermal evolution models of asteroids. In: Bottke Jr., W.F., Cellino, A., Paolicchi, P., Binzel, R.P. (Eds.), Asteroids III. The University of Arizona Press, Tucson, pp. 559–571.

Meibom, A., Clark, B.E., 1999. Evidence for the insignificance of ordinary chondritic material in the asteroid belt. Meteorit. Planet. Sci. 34, 7–24.

Mittlefehldt, D.W., McCoy, T.J., Goodrich, C.A., Kracher, A., 1998. Nonchondritic meteorites from asteroidal bodies. In: Papike, J.J. (Ed.), Planetary Materials, vol. 36. Mineralogical Society of America, Washington, pp. 4-1–4-195.

Molin, G.M., 1989. Crystal–chemical study of cation disordering in Al-rich and Al-poor orthopyroxenes from spinel lherzolite xenoliths. Am. Mineral. 74, 593–598.

Motohara, K., Iwamuro, F., Maihara, T., Oya, S., Tsukamoto, H., Imanishi, M., Terada, H., Goto, M., Iwai, J., Tanabe, H., Hata, R., Taguchi, T., Harashima, T., 2002. CISCO: Cooled infrared spectrograph and camera for OHS on the Subaru telescope. Publ. Astron. Soc. Pac. Jpn. 54, 315–325.

Moroz, L., Schade, U., Wasch, R., 2000. Reflectance spectra of olivine–orthopyroxene-bearing assemblages at decreased temperatures: Implications for remote sensing of asteroids. Icarus 147, 79–93.

Nord Jr., G.L., 1980. The composition, structure, and stability of Guinier–Preston zones in lunar and terrestrial orthopyroxene. Phys. Chem. Miner. 6, 109–128.

Papike, J.J., 1987. Chemistry of the rock-forming silicates: Ortho, ring, and single-chain structures. Rev. Geophys. 25, 1483–1526.

Pasqual, D., Molin, G., Tribaudino, M., 2000. Single-crystal thermometric calibration of Fe–Mg order–disorder in pigeonites. Am. Mineral. 85, 953–962.

Rayner, J.T., Toomey, D.W., Onaka, P.M., Denault, A.J., Stahlberger, W.E., Vacca, W.D., Cushing, M.C., Wang, S., 2003. SpeX: A medium-resolution 0.8–5.5 micron spectrograph and imager for the NASA infrared telescope facility. Publ. Astron. Soc. Pac. 115, 362–382.

Rayner, J.T., Onaka, P.M., Cushing, M.C., Vacca, W.D., 2004. Four years of good SpeX. SPIE 5492, 1498–1509.

Reed, K.L., Gaffey, M.J., Lebofsky, L.A., 1997. Shape and albedo variations of Asteroid 15 Eunomia. Icarus 125, 446–454.

Reddy, V., Hardersen, P.S., Gaffey, M.J., Abell, P.A., 2005. Mineralogy and temperature-induced spectral investigations of A-type Asteroids 246 Asporina and 446 Aeternitas. Lunar Planet. Sci. 36. Abstract 1375.

Rivkin, A.S., Binzel, R.P., Sunshine, J., Bus, S.J., Burbine, T.H., Saxena, A., 2004. Infrared spectroscopic observations of 69230 Hermes (1937 UB): Possible unweathered endmember among ordinary chondrite analogs. Icarus 172, 408–414.

Ross, N.L., Sowerby, J.R., 1996. Crystal field spectrum of synthetic clinoferrosilite. In: Dyar, M.D., McCammon, C., Schafer, M.W. (Eds.), Mineral Spectroscopy: A Tribute to Roger G. Burns. Geochemical Society, St. Louis, pp. 273–280.

Rossman, G.R., 1980. Pyroxene spectroscopy. In: Prewitt, C.T. (Ed.), Pyroxenes, vol. 7. Mineralogical Society of America, Washington, pp. 93–115.

Sasaki, T., Sasaki, S., Watanabe, J., Sekiguchi, T., Yoshida, F., Kawakita, H., Fuse, T., Takato, N., Dermawan, B., Ito, T., 2004. Mature and fresh surfaces on the newborn Asteroid Karin. Astrophys. J. 615, L161–L164.

Saxena, S.K., Tazzoli, V., Domeneghetti, M.C., 1987. Kinetics of Fe^{2+}–Mg distribution in aluminous orthopyroxenes. Phys. Chem. Miner. 15, 140–147.

Schade, U., Wasch, R., Moroz, L., 2004. Near-infrared reflectance spectroscopy of Ca-rich clinopyroxenes and prospects for remote spectral characterization of planetary surfaces. Icarus 168, 80–92.

Schlenz, H., Kroll, H., Phillips, M.W., 2001. Isothermal annealing and continuous cooling experiments on synthetic orthopyroxenes: Temperature and time evolution of the Fe, Mg distribution. Eur. J. Mineral. 13, 715–726.

Shimazu, H., Terasawa, T., 1995. Electromagnetic induction heating of meteorite parent bodies by the primordial solar wind. J. Geophys. Res. 100 (E8), 16923–16930.

Singer, R.B., 1981. Near-infrared spectral reflectance of mineral mixtures: Systematic combinations of pyroxenes, olivine, and iron oxides. J. Geophys. Res. 86 (B9), 7967–7982.

Sunshine, J.M., Bus, S.J., McCoy, T.J., Burbine, T.H., Corrigan, C.M., Binzel, R.P., 2004. High-calcium pyroxene as an indicator of igneous differentiation in asteroids and meteorites. Meteorit. Planet. Sci. 39, 1343–1357.

Tarantino, S.C., Domeneghetti, M.C., Carpenter, M.A., Shaw, C.J.S., Tazzoli, V., 2002. Mixing properties of the enstatite–ferrosilite solid solution. I. A macroscopic perspective. Eur. J. Mineral. 14, 525–536.

Tedesco, E.F., Noah, P.V., Noah, M., Price, S.D., 2002. The supplemental IRAS minor planet survey. Astron. J. 123, 1056–1085.

Tholen, D.J., 1984. Asteroid taxonomy from cluster analysis of photometry. PhD thesis. University of Arizona, Tucson.

Tholen, D.J., Barucci, M.A., 1989. Asteroid taxonomy. In: Binzel, R.P., Gehrels, T., Matthews, M.S. (Eds.), Asteroids II. The University of Arizona Press, Tucson, pp. 298–315.

Tholen, D.J., 1999. Ephem. Version 1.2. Celestech.

Urey, H.C., 1955. The cosmic abundances of potassium, uranium, and thorium and the heat balances of the Earth, the Moon, and Mars. Proc. Natl. Acad. Sci. 41, 127–144.

Vacca, W.D., Cushing, M.C., Rayner, J.T., 2004. Nonlinearity corrections and statistical uncertainties associated with near-infrared arrays. Publ. Astron. Soc. Pac. 116, 352–361.

Wang, X.B., Shi, Y., 2002. CCD photometry of Asteroids 38, 174, 276 and 346. Earth Moon Planet. 1991, 181–186.

Xu, S., Binzel, R.P., Burbine, T.H., Bus, S.J., 1995. Small main-belt asteroid spectroscopic survey: Initial results. Icarus 115, 1–35.

Zema, M., Tarantino, S.C., Domeneghetti, M.C., Tazzoli, V., 2003. Ca in orthopyroxene: Structural variations and kinetics of the disordering process. Eur. J. Mineral. 15, 373–380.